FLOW CAMBRIDGE UNIVERSITY PRESS

RESEARCH ARTICLE

Theoretical modelling of the three-dimensional wake of vertical axis turbines

Pablo Ouro[1,2,*] (ORCID) and Maxime Lazennec[3]

[1]School of Mechanical, Aerospace and Civil Engineering, University of Manchester, Manchester M13 9PL, UK
[2]Hydro-environmental Research Centre, School of Engineering, Cardiff University, The Parade, Cardiff CF24 3AA, UK
[3]École Polytechnique, Paris, 91120 Palaiseau, France
*Corresponding author. E-mail: pablo.ouro@manchester.ac.uk

Abstract

Vertical axis turbine (VAT) arrays can achieve larger power generation per land area than their horizontal axis counterparts, due to the positive synergy from clustering VATs in close proximity. The VATs generate a three-dimensional wake that evolves unevenly over the vertical and transverse directions according to two governing length scales, namely the rotor's diameter and height. Theoretical wake models need to capture such a complex wake dynamics to enable reliable array design that maximises energy output. This paper presents two new theoretical VAT wake models based on super-Gaussian and Gaussian shape functions, which account for the three-dimensional velocity deficit distribution in the wake. The super-Gaussian model represents the initial elliptical shape with the superposition of vertical and lateral shape functions that progressively converge into an axisymmetric circular-shaped wake at a downstream distance that depends on the rotor's height-to-diameter aspect ratio. Our Gaussian model improves the initial wake width prediction taking into account the rectangular rotor's cross-section. Our models were well validated with large-eddy simulations (LES) of single VATs with varying aspect ratios and thrust coefficients operating in an atmospheric boundary layer. The super-Gaussian model attained a good agreement with LES in both near and far wake, whilst the Gaussian model represented well the far-wake region.

Impact Statement

The efficient design of wind or hydro-kinetic turbine arrays requires the analysis of multiple layouts for a range of flow conditions, with the goal of maximising the energy yield over the project lifespan. This process can be accomplished adopting analytical wake models as they provide a reasonable accuracy to predict the velocity field accounting for wake-to-wake interactions, as well as having a low computational overhead enabling layout optimisation. As power scales to the cube of velocities, i.e. $P \propto U^3$, it is of utmost importance to develop wake models that represent accurately the wakes downstream of turbines. This paper introduces a new super-Gaussian and Gaussian wake models for vertical axis turbines (VATs) capable of capturing the three-dimensional shape and maximum velocity deficit of their wake, notably improving any existing VAT wake model. The adoption of these theoretical models for array design by industry and researchers will enable more reliable estimates of the optimal turbine spacing that maximise the energy yield, contributing to accelerate the development of this technology for renewable energy generation.
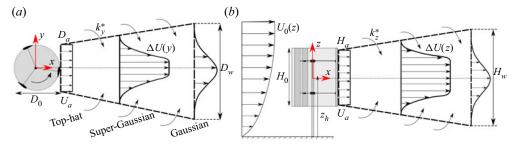
CrossMark

1. Introduction

In the global landscape of wind energy generation, all commercial-scale onshore and offshore wind farm projects comprise horizontal axis turbines (HATs) as a well established technology. Vertical axis turbines (VATs) are being developed at a slower pace with a remaining main challenge to prove their financial viability in large-scale projects, which is partly conditioned by the need to enhance their energy generation capabilities. The VATs offer a series of advantages over their HAT counterparts that can lead to innovative wind and hydro-kinetic energy projects, e.g. they can effectively harness energy from low-to-medium flow velocity ranges such as found in urban areas, rivers or tides, or be adopted in environmentally sensitive regions as their slower rotational speeds can reduce fish collision risk and noise (Castro-Santos & Haro, 2013).

The VAT rotor blades rotate with their rotational axis perpendicular to the incident flow direction, generating vortical structures during the upstroke rotation and interacting with these over the downstroke period. This complex flow dynamics depends on the operational regime accounted for by the tip-speed ratio (TSR), which relates the blades' angular speed to the free-stream velocity; and the turbine's rotor geometric solidity, which indicates the proportion of swept perimeter occupied by the blades (Posa, 2020b). The VATs designed with low-solidity rotors operate at high TSR with the blades undergoing light dynamic stall, i.e. flow separation occurs for effective angles of attack larger than the static-stall angle. In contrast, rotors with higher solidity operate at low TSR and blades experience deep dynamic stall, meaning that leading-edge vortices enhance the blades' lift-generation capability but eventually get fully detached originating a sudden drop in lift and torque, thus triggering large load fluctuations (Ouro & Stoesser, 2017).

Despite the complex fluid–structure interaction, there is limited research looking into the governing flow mechanics of VAT wakes, especially in the far-wake region (Posa, 2020a). Most experimental tests of VATs look at how to improve their performance, leading to a limited number of studies analysing the near-wake flow field and fewer extensive tests investigating the far wake. Particularly for the latter, only a few small-scale laboratory studies exist, including: Rolin & Porté-Agel (2018) measured with particle image velocimetry (PIV) up to 10 diameters (D_0) downstream of a VAT analysing the mean and turbulent kinetic energy equations; Araya et al. (2017) investigated the near- to far-wake transition for turbine rotors with different number of blades and TSRs using PIV to measure up to $11D_0$ downstream; and Ouro et al. (2019) measured the wake up to $14D_0$ downstream with an acoustic Doppler velocimeter, showing that remnants of the turbine-induced wake are still observed at such far distances downstream.

The uneven, three-dimensional distribution of VAT wakes is depicted in Figure 1, which considers a control volume (thick black lines) behind a turbine of diameter D_0 and height H_0 in which mass and momentum need to be conserved (Bastankhah & Porté-Agel, 2014). Over the horizontal xy-plane, the main contribution to momentum entrainment over the lateral boundaries of the control volume results from blade-induced energetic vortices (Kadum et al., 2018). This differs from the wake recovery dynamics over the xz-vertical plane (Figure 1b), as shear layers generated over this direction result from tip vortices (Tescione et al., 2014). These blade-induced structures are not identical, contributing to a highly three-dimensional wake (Ouro et al., 2019). Figure 1 shows that VAT rotors have two length scales that characterise the wake shape, namely D_0 is the characteristic length scale in the horizontal xy-plane while in the vertical xz-plane this is H_0.

More insights into the complex turbulent structures generated by VAT rotor blades were gained from numerical simulations. Previous research has evidenced the need for eddy-resolving closures, e.g. large-eddy simulation (LES), to resolve this highly turbulent flow in order to capture dynamic stall (Ouro et al., 2018) and estimate how turbulence drives the kinetic energy replenishment in the wake (Bachant & Wosnik, 2016; Ouro et al., 2019; Posa, 2020a). Geometry-resolved simulations provided of high grid resolutions at the rotor can capture the vortices induced by the blades (Posa & Balaras, 2018; Ouro & Stoesser, 2017). Actuator techniques capture the main wake dynamics while adopting coarser resolutions (Porté-Agel et al., 2020), with the actuator line model (ALM) being the most adopted one

Figure 1. *Velocity deficit (ΔU) field behind a VAT of diameter D_0 and height H_0 over the (a) horizontal xy-plane at a mid-height elevation ($z = z_h$) from the ground level, and (b) vertical xz-plane through the rotor's centre (y = 0). Here, k_y^* and k_z^* are the wake expansion rates. Thick solid lines denote the control volume in which mass and momentum are conserved.*

(Shamsoddin & Porté-Agel, 2016; Abkar & Dabiri, 2017; Mendoza et al., 2019), although an improved resolution of the flow at rotor level can be obtained with actuator surface models (Massie et al., 2019).

The drawback of high-fidelity LES–ALM is its large computational expense, becoming unfeasible to design array layouts (Hezaveh et al., 2018). Alternatively, analytical wake models represent the wake shape, normally adopting a top-hat, Gaussian or super-Gaussian distribution, enabling the optimisation of array layouts that provide the best performance throughout the project's lifespan (Stansby & Stallard, 2016; Shapiro et al., 2019). The adopted model needs to capture the velocity and length scales that define the wake in order to improve the results and diminish the uncertainty in the predictions (Archer et al., 2018). For instance, for HAT wakes Gaussian shape functions provide good results for HATs with zero yaw angle as their wakes feature an axisymmetric distribution, allowing us to consider the velocity deficit field to be self-similar (Stallard et al., 2015; Bastankhah & Porté-Agel, 2016). Recent wake models adopting super-Gaussian functions have been introduced for HATs, providing good results, especially in the near wake compared to standard Gaussian models. The former have an initial shape close to a top-hat distribution behind the turbine and evolve towards a nearly Gaussian shape further downstream (Shapiro et al., 2019; Blondel & Cathelain, 2020).

In the case of VATs, there is still a need for developing analytical wake models that can describe and predict the three-dimensional field (Meneveau, 2019), as the wake is three-dimensional and scales with the VAT rotor's diameter and height, unlike HAT wakes that scales with the diameter. Current theoretical VAT wake models do not account for the uneven wake expansion over the horizontal and vertical planes (Figure 1), and represent its shape with standard Gaussian functions (Abkar & Dabiri, 2017; Abkar, 2019). To overcome these limitations, a super-Gaussian shape enables a more physically realistic description of the VAT wake velocity field compared to top-hat models that assume a uniform value across the wake or Gaussian models that fail to reproduce the elliptical shape (Blondel & Cathelain, 2020).

We present and validate two novel analytical models based on a new super-Gaussian function and an improved model that adopts a Gaussian function. The former is particularly suitable for VAT wakes as it enables us to represent the near wake with an almost top-hat distribution which evolves towards a nearly Gaussian shape in the far wake. It captures the elliptical wake shape with the superposition of two different super-Gaussian functions in the lateral and vertical directions. We also propose a Gaussian wake model that improves the initial wake width, overcoming the limitation found in previous VAT wake models to calculate the velocity deficit in the near-wake region. Our models are applicable to wind vertical axis turbines in zero-pressure flows and also to hydro-kinetic VATs if these operate in a boundless environment without considerable influence from free-surface proximity or channel lateral blockage (Ross & Polagye, 2020). For simplicity, we refer to either of these as VATs to generalise the models' applicability.

2. Derivation of the Wake Models

2.1. Momentum Conservation

We build our momentum conserving wake models starting from the conservation form of the Reynolds-averaged Navier–Stokes (RANS) equations for high Reynolds numbers in the streamwise direction. After neglecting viscous terms and considering the wakes to be in zero-pressure gradient flow, e.g. not in a high blockage environment as a shallow tidal channel, the equation reads

$$\frac{\partial U_w(U_0 - U_w)}{\partial x} + \frac{\partial V_w(U_0 - U_w)}{\partial y} + \frac{\partial W_w(U_0 - U_w)}{\partial z} = \frac{\partial u'u'}{\partial x} + \frac{\partial u'v'}{\partial y} + \frac{\partial u'w'}{\partial z}, \tag{1}$$

with (U_w, V_w, W_w) being the vector of mean wake velocities in the streamwise, transverse and vertical directions respectively, U_0 is the free-stream velocity and $u'u'$, $u'v'$ and $u'w'$ denote time-averaged turbulent fluctuation correlations. We integrate (1) at any streamwise location of a control volume that embeds the turbine and expands over the y and z directions from $-\infty$ to ∞, which together with the assumption that the shear stresses vanish when the distance from the wake centre increases, provides the resulting RANS equation:

$$\frac{\mathrm{d}}{\mathrm{d}x} \int_{-\infty}^{\infty} (U_w(U_0 - U_w) - u'u') \, \mathrm{d}A \approx 0. \tag{2}$$

The streamwise variation of $u'u'$ is much reduced when compared to the convective term (Bastankhah & Porté-Agel, 2014), hence (2) can be simplified to obtain the momentum integral (Tennekes & Lumley, 1972) as

$$\rho \int_{-\infty}^{\infty} (U_w(U_0 - U_w)) \, \mathrm{d}A = T. \tag{3}$$

This equilibrium condition states that the momentum deficit flux in the wake is proportional to the thrust force T exerted by the turbine. The thrust force can be related to the thrust coefficient (C_T) from the actuator disc theory as

$$T = \tfrac{1}{2} C_T \rho A_0 U_0^2. \tag{4}$$

where ρ indicates the fluid density.

2.2. Top-hat Wake Distribution

Analogously to the Frandsen et al. (2006) top-hat HAT wake model, we assume the distance downstream of the rotor the flow in the wake required to reach the free-flow pressure is negligible. The cross-sectional area of the wake just after the initial wake expansion is considered rectangular as the turbine rotor's cross-sectional area at $x = x_a$, i.e. $A_w(x_a) = A_a$. The value of the wake onset area A_a can be determined using the actuator disc theory as $A_a = \beta A_0$, with β representing the relative initial wake expansion at $x_a = 0$ in terms of the turbine rotor's cross-section A_0, independently of whether such cross-section is circular (HATs) or rectangular (VATs). For a C_T lower than the unity, the actuator disc theory states that the velocity over the plane at a downstream distance x_a is $U_0(1 - 2a)$ whilst at the rotor centre plane the velocity is $U_0(1 - a)$, with $a = (1 - \sqrt{1 - C_T})/2$ being the so-called induction factor. Hence, the value of β is determined as

$$\beta = \frac{A_a}{A_0} = \frac{1 - a}{1 - 2a} = \frac{1}{2} \frac{1 + \sqrt{1 - C_T}}{\sqrt{1 - C_T}}. \tag{5}$$

The wake area at any streamwise location is determined similarly to the approach presented by Frandsen et al. (2006) for HATs with $D_w \propto (x - x_a)^{1/2}$ and $H_w \propto (x - x_a)^{1/2}$, considering the wake

width expands unevenly over the horizontal and vertical directions according to

$$D_w = D_0 \left(\beta + k_{w_y} \frac{x}{D_0}\right)^{1/2}, \quad H_w = H_0 \left(\beta + k_{w_z} \frac{x}{H_0}\right)^{1/2}. \tag{6}$$

We now apply momentum balance to a control volume that embeds the operating turbine expanding some distance upstream and downstream to obtain the velocity deficit ($\Delta U = U_0 - U_w$) for the top-hat model with an uneven expansion over the horizontal and vertical directions

$$\frac{\Delta U}{U_0} = \frac{1}{2} \left(1 - \sqrt{1 - \frac{2C_T}{\left(\beta + k_{w_y} \frac{x}{D_0}\right)^{1/2} \left(\beta + k_{w_z} \frac{x}{H_0}\right)^{1/2}}}\right). \tag{7}$$

Values of k_{w_y} and k_{w_z} are the wake expansion rates in the y- and z-directions respectively, which can be calculated as $2.0 I_u$ with $I_u = (u'u')^{0.5}/U_0$ being the streamwise turbulence intensity (Frandsen et al., 2006). In our study, we derived this top-hat wake model to estimate the initial wake width in the super-Gaussian and Gaussian models.

2.3. Super-Gaussian and Gaussian Wake Models

In the derivation of a super-Gaussian model, the wake is assumed to feature a velocity deficit (ΔU) distribution that evolves in the streamwise direction according to the local scale of velocity $C(x)$, determined as the maximum normalised velocity deficit ($\Delta U_{max}/U_0$); and spatial length scales $f_y(y)$ and $f_z(z)$ that define an three-dimensional super-Gaussian distribution according to exponents n_y and n_z, respectively. In the case of HATs (Blondel & Cathelain, 2020) or VATs, the wake starts with a rectangular (or nearly top-hat) shape immediately and evolves with an elliptical shape until attaining a Gaussian shape in the far wake ($n_y = n_z = 2$) assuming it is self-similar (Bastankhah & Porté-Agel, 2014). Thus, n_y and n_z are deemed to vary in the streamwise direction following an exponential decay as

$$n_y = a_y \exp\left(-b_y \frac{x}{D_0}\right) + c_y, \quad n_z = a_z \exp\left(-b_z \frac{x}{H_0}\right) + c_z. \tag{8}$$

Here, we denote the normalised local coordinates $\tilde{y} = (y - y_c)/D_0$ and $\tilde{z} = (z - z_c)/H_0$, with $y_c = 0$ and $z_c = z_h$ being the centre of the turbine's rotor (Figure 1). Our super-Gaussian model is derived considering an uneven evolution of the wake shape over the y- and z-directions, i.e. $a_y \neq a_z$ and $b_y \neq b_z$ as shown later in § 4. Note that, in (8), we propose that the evolution of the shape exponent over the y-direction scales with D_0 whilst in the vertical direction this is with H_0. The evolution of ΔU according to the superposition of super-Gaussian shapes f_y and f_z can be estimated as

$$\frac{\Delta U}{U_0} = \frac{U_0 - U_w}{U_0} = C(x) \exp\left(-\frac{\tilde{y}^{n_y}}{2\tilde{\sigma}_y^2}\right) \exp\left(-\frac{\tilde{z}^{n_z}}{2\tilde{\sigma}_z^2}\right). \tag{9}$$

The characteristic wake widths σ_y and σ_z again scale depending on D_0 and H_0, respectively, i.e. $\tilde{\sigma}_y = \sigma_y/D_0$ and $\tilde{\sigma}_z = \sigma_z/H_0$. These wakes grow linearly in the downstream direction according to the wake expansion rates k_y^* and k_z^* respectively, which read

$$\tilde{\sigma}_y = k_y^* \frac{x}{D_0} + \varepsilon_y, \quad \tilde{\sigma}_z = k_z^* \frac{x}{H_0} + \varepsilon_z, \tag{10}$$

with ε_y and ε_z representing the initial wake expansion at x_a. In our model, the wake expansion rates are determined as a function of the streamwise turbulence intensity as $k_y^* = k_z^* = 0.45 I_u$, which are slightly greater than the values normally adopted for HAT. The wake velocity deficit (9) can be re-written as

$$U_w = U_0 \left[1 - C(x) \exp\left(-\frac{\tilde{y}^{n_y}}{2\tilde{\sigma}_y{}^2}\right) \exp\left(-\frac{\tilde{z}^{n_z}}{2\tilde{\sigma}_z{}^2}\right) \right].$$ (11)

We need to determine the velocity scale $C(x)$ as the unknown variable from this algebraic equation. Considering the wake area to be $A_w = D_w H_w$ ($dA = dy\,dz$) depicted in Figure 1, we equate the momentum integral (3) to the turbine thrust force (4) to obtain the definition of the wake velocity (11) as

$$\int_{-\infty}^{\infty} \int_{-\infty}^{\infty} C(x) \exp\left(-\frac{\tilde{y}^{n_y}}{2\tilde{\sigma}_y{}^2} - \frac{\tilde{z}^{n_z}}{2\tilde{\sigma}_z{}^2}\right) \left[1 - C(x) \exp\left(-\frac{\tilde{y}^{n_y}}{2\tilde{\sigma}_y{}^2} - \frac{\tilde{z}^{n_z}}{2\tilde{\sigma}_z{}^2}\right) \right] dy\,dz = \frac{1}{2} C_T A_0.$$ (12)

In the integration of (12) we consider that $\int_{-\infty}^{\infty} \exp(-\tilde{y}^{n_y}/(2\tilde{\sigma}_y{}^2))\,dy = 2/n_y D_0 \Gamma(1/n_y)(2\tilde{\sigma}_y{}^2)^{1/n_y}$, $\int_{-\infty}^{\infty} \exp(-\tilde{y}^{n_y}/\tilde{\sigma}_y{}^2)\,dy = 2/n_y D_0 \Gamma(1/n_y)\tilde{\sigma}_y{}^{2/n_y}$, and analogously for the integrals in z-direction, with $\Gamma(1/2) = \sqrt{\pi}$ and $\Gamma(1) = 1$. For convenience, from hereafter we denote $\eta = 1/n_y + 1/n_z$. Equation (12) can be integrated to determine the normalised maximum velocity deficit, $C(x)$, as

$$C(x)^2 - C(x)2^\eta + \frac{C_T n_y n_z}{8\tilde{\sigma}_y{}^{2/n_y} \tilde{\sigma}_z{}^{2/n_z} \Gamma(1/n_y)\Gamma(1/n_z)} = 0.$$ (13)

From the two possible roots of this quadratic equation, the solution that provides a physically acceptable value for the characteristic velocity scale is

$$C(x) = 2^{\eta-1} - \sqrt{2^{2\eta-2} - \frac{C_T n_y n_z}{8\tilde{\sigma}_y{}^{2/n_y} \tilde{\sigma}_z{}^{2/n_z} \Gamma(1/n_y)\Gamma(1/n_z)}}.$$ (14)

Hence, our super-Gaussian model for VAT wakes is determined from (11) and (14) as

$$\frac{\Delta U}{U_0} = \left(2^{\eta-1} - \sqrt{2^{2\eta-2} - \frac{C_T n_y n_z}{8\tilde{\sigma}_y{}^{2/n_y} \tilde{\sigma}_z{}^{2/n_z} \Gamma(1/n_y)\Gamma(1/n_z)}} \right) \left[\exp\left(-\frac{\tilde{y}^{n_y}}{2\tilde{\sigma}_y{}^2}\right) \exp\left(-\frac{\tilde{z}^{n_z}}{2\tilde{\sigma}_z{}^2}\right) \right].$$ (15)

Note that if a Gaussian velocity profile is considered for both f_y and f_z, i.e. $n_y = n_z = 2$, then $\tilde{y}^2/\tilde{\sigma}_y{}^2 = y^2/\sigma_y^2$ and $\tilde{z}^2/\tilde{\sigma}_z{}^2 = z^2/\sigma_z^2$, yielding a velocity deficit expression

$$\frac{\Delta U}{U_0} = \left(1 - \sqrt{1 - \frac{C_T A_0}{2\pi\sigma_y\sigma_z}} \right) \left[\exp\left(-\frac{y^2}{2\sigma_y{}^2}\right) \exp\left(-\frac{z^2}{2\sigma_z{}^2}\right) \right].$$ (16)

2.3.1. Initial Wake Width
We need to determine the initial wake width to estimate the values of ε_y and ε_z adopted in the calculation of the wake widths $\tilde{\sigma}_y$ and $\tilde{\sigma}_z$. These are determined from the mass flow deficit rate ($m = \rho \iint \Delta U \, dA$, with ρ being the density of the fluid) immediately behind the turbine's rotor $x = 0$, equating the prediction from the momentum-conserving top-hat model (7) to the value from the super-Gaussian model (15), which ensures mass and momentum are conserved over the wake width. The expression of

Table 1. *Details of the parameters adopted in the super-Gaussian and Gaussian wake models.*

Model	a_y	a_z	b_y	b_z	c_y	c_z	k_y^*	k_z^*
Super-Gaussian	0.95	4.5	0.35	0.70	2.4	2.4	$0.50I_u$	$0.50I_u$
Gaussian	—	—	—	—	2.0	2.0	$0.35I_u$	$0.35I_u$

mass flow deficit rate for the super-Gaussian wake model reads

$$
m_{SG} = \left(2^{\eta-1} - \sqrt{2^{2\eta-2} - \frac{C_T n_y n_z}{8\varepsilon_y^{2/n_y}\varepsilon_z^{2/n_z}\Gamma(1/n_y)\Gamma(1/n_z)}} \right) \frac{D_0 H_0 2^{\eta+2}\varepsilon_y^{2/n_y}\varepsilon_z^{2/n_z}\Gamma(1/n_y)\Gamma(1/n_z)}{n_y n_z}.
$$

(17)

Alternatively, the mass flow deficit rate from the top-hat model (7) is

$$
m_{TH_{x=0}} = \left(1 - \sqrt{1 - \frac{2C_T}{\beta}} \right) \frac{D_a H_a}{2}.
$$

(18)

Considering the wake onset widths ε_y and ε_z are equal to ε, we obtain

$$
\varepsilon(n_{y,z} \geq 2) = \left(\frac{\beta n_y n_z}{2^{2\eta+2}\Gamma(1/n_y)\Gamma(1/n_z)} \right)^{1/(2\eta)}.
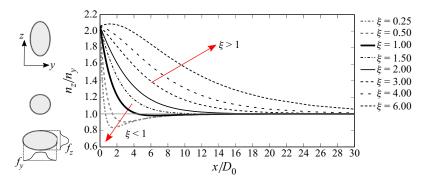$$

(19)

It should be noted that these values of n_y and n_z are those at $x = 0$, as ε_y and ε_z are solely evaluated as the initial wake width. The initial wake width adopting a Gaussian distribution is

$$
\varepsilon(n_{y,z} = 2) = \sqrt{\frac{\beta}{4\pi}}.
$$

(20)

The initial wake expansion rates are just a function of β, i.e. only depend on the thrust coefficient C_T. It is noteworthy that our estimation of the initial wake width using a super-Gaussian model (19) differs from the definition $\varepsilon = \sqrt{\beta}/4$ proposed by Abkar & Dabiri (2017) which is approximately 12% smaller and corresponds to the value used in HAT wake models. Our formulation overcomes limitations derived from an inaccurate definition of ε which can yield non-physical estimations of the velocity deficit at short distances behind the turbines. Furthermore, the velocity scale obtained in our Gaussian model (16) differs from that proposed in Abkar & Dabiri (2017), as the latter assumed the velocity deficit at the wake onset to be that of HATs (Bastankhah & Porté-Agel, 2014), while our theoretical framework is derived considering the rectangular section of VAT rotors. This consideration, together with the initial wake width (20), allows us to compute the velocity deficit field at any downstream location for any C_T and rotor aspect ratio. In Table 1 we present the values of the super-Gaussian wake model (19) parameters, which provided the lowest error in the velocity predictions, and wake recovery rates used in the Gaussian model. The computed root-mean-square error in the velocity predictions shown later in Section 4 varied less than 2% when decreasing or increasing the super-Gaussian model input parameters a_y, a_z, b_y and b_z by ±20%, similarly to the sensitivity analysis presented in Abkar (2019) for a Gaussian model.

3. Evolution of the Wake Shape with Varying Aspect Ratio

A key aspect that can be elucidated with our three-dimensional super-Gaussian model is whether VAT wakes ever become circular (i.e. axisymmetric) and, if so, at what distance downstream the turbine is this accomplished? The evolution from an elliptical shape converging into a circular one was observed by Shamsoddin & Porté-Agel (2020) using LES for three rotor aspect ratios. According to (8), the evolution

Figure 2. *Evolution of wake shape accounted for by the ratio n_z/n_y, with schematics of the wake shape on the left-hand side.*

of the shape function exponents n_y and n_z scale with D_0 and H_0 respectively, thus the downstream distance at which symmetry in the wake shape is accomplished depends on the aspect ratio $\xi = H_0/D_0$. This is irrespective of the wake recovery rate that is a linear function of k_y^* and k_z^*, which are both equal and only a function of turbulence intensity (Table 1).

We present the downstream evolution of the ratio n_z/n_y for different aspect ratios in Figure 2 to identify whether the wake shape is elliptical (asymmetric) or circular (i.e. $n_z=n_y$). As presented in Figure 11 in the Appendix, at the wake onset, the exponents $n_y(x = 0)$ and $n_z(x = 0)$ approach 3.35 and 6.9 respectively, representing top-hat-like shape functions, yielding an initial value $n_z/n_y(x = 0)$ equal to 2.060. Further downstream these eventually converge towards a value of 2.4, i.e. $n_z/n_y = 1.0$, similarly to other HAT super-Gaussian models (Shapiro et al., 2019; Blondel & Cathelain, 2020). For a square-shaped rotor, i.e. $\xi = 1$, the near wake is characterised by n_z being larger than n_y until $x/D_0 \approx 4.0$, when a reversed shape is developed, and not until approximately $10D_0$ is a symmetric (circular) wake recovered. For $\xi \geq 1.5$, the ratio n_z/n_y remains larger than 1.0 at all streamwise distances, indicating that the wake requires a longer streamwise distance to recover the Gaussian shape over the vertical direction that in the lateral one. Thus, increasing the aspect ratio progressively increases the downstream distance required to recover wake symmetry, and for $\xi \geq 5.0$ the maxima of the n_z/n_y ratio are not attained at the wake onset but instead at some distance downstream x up to which n_z evolves notably slower than n_y (Figure 11). Conversely, for $\xi \leq 1.5$ the asymmetry in the near wake comes from f_z evolving faster towards a nearly Gaussian distribution than f_y, with the circular shape attained after approximately 10–12D_0, equivalent to $64H_0$ for $\xi = 0.25$. Our super-Gaussian theoretical model indicates that a symmetric circular shape is recovered fastest with $\xi = 1.5$ (specifically at $x/D_0 = 10$), as this is the threshold value at which the wake in the vertical direction never approaches the Gaussian shape at a faster rate than over the horizontal plane.

4. Validation of the Wake Models

We validate our theoretical wake models in six cases comprising a single VAT operating in the turbulent atmospheric boundary layer flow with comparisons to high-fidelity LES. Cases 1a, 1b and 1c reproduce the LES from Shamsoddin & Porté-Agel (2020) which change the turbine rotor's aspect ratio (ξ) from 2.0 to 0.25, whilst keeping the incident flow characteristics and turbine operation constant. Cases 2a and 2b consider the set-up and LES results presented in Abkar & Dabiri (2017) in which the VAT rotor's diameter and height are kept constant ($\xi = 0.92$) but thrust coefficients are lower than in cases 1a to 1c. For completeness, case 2c is also included despite its aspect ratio is close to case 1b but the thrust coefficient is smaller. These benchmarks are selected as they provide the necessary information to input in the analytical models, i.e. approach velocity characteristics (e.g. free-stream velocity, U_0, and turbulence intensity, I_u), rotor dimensions and, more importantly, thrust coefficient (see Table 2

Table 2. *Details of the cases tested, including VAT rotor's diameter D, height H and aspect ratio ξ, height above ground of the turbine's centre z_h, thrust coefficient C_T, free-stream velocity U_0, streamwise turbulence intensity I_u and TSR λ.*

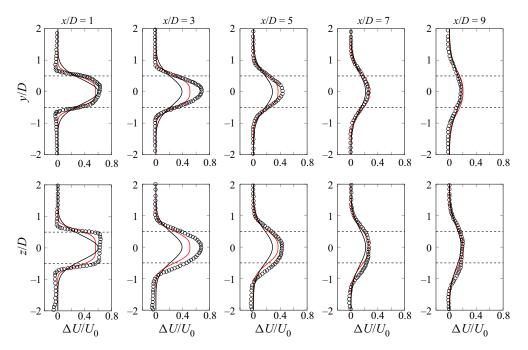| Case	D (m)	H (m)	ξ (−)	z_h (m)	C_T (−)	U_0 (m s^{-1})	I_u (−)	λ (−)
1a	50	50	1.00	100	0.80	9.6	0.083	4.5
1b	50	100	2.00	100	0.80	9.6	0.083	4.5
1c	50	12.5	0.25	100	0.80	9.6	0.083	4.5
2a	26	24	0.92	40	0.64	7.0	0.091	3.8
2b	26	24	0.92	40	0.34	7.0	0.091	2.5
2c	26	48	1.85	40	0.64	7.0	0.091	3.8

Figure 3. *Normalised velocity deficit profiles for case 1a with $C_T = 0.80$ and $\xi = 1.0$. Comparison of our proposed super-Gaussian (red line) and Gaussian (black line) analytical wake models, with LES results from* Shamsoddin & Porté-Agel (2020) *(circles).*

for details). Hereafter, the origin of coordinates is at the turbine rotor's centre of rotation and mid-height, and for simplicity the turbine rotor's diameter and height are represented by D and H instead of D_0 and H_0.

4.1. *Case 1: VAT of Varying Aspect Ratio from Shamsoddin & Porté-Agel (2020)*

Our super-Gaussian and Gaussian theoretical wake models are firstly validated for the three full-scale VATs of different aspect ratio originally presented in Shamsoddin & Porté-Agel (2020) which used LES–ALM. The approach flow follows a logarithmic distribution with a roughness height of 0.1 m and friction velocity equal to 0.52 m s^{-1} (Shamsoddin & Porté-Agel, 2016). In Figure 3 we present the horizontal (y) and vertical (z) profiles of the normalised velocity deficit, ΔU, at streamwise locations $x/D = 1, 3, 5, 7$ and 9 for case 1a ($\xi = 1.0$). There is a notable three-dimensionality in the near wake at
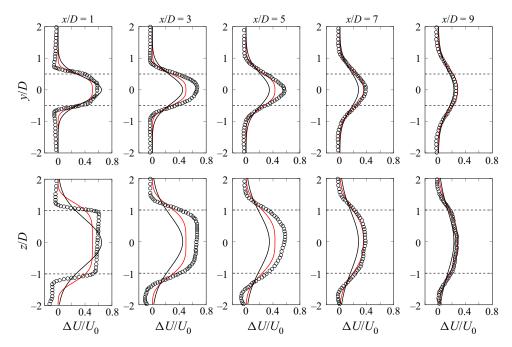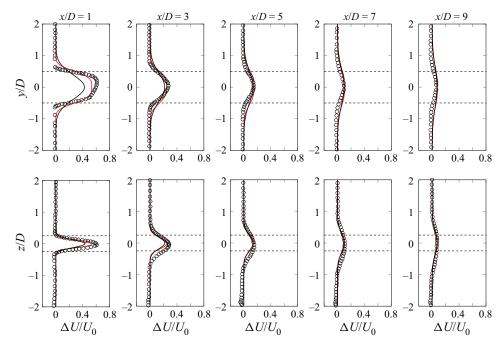
Figure 4. *Normalised velocity deficit profiles for case 1b with C_T = 0.80 and ξ = 2.0. Same legend as* Figure 3.
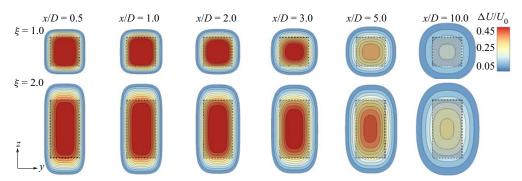
$x/D = 1$, with the vertical profile featuring a top-hat-like shape whilst the wake shape in the y-direction is closer to a Gaussian distribution. Here, the super-Gaussian wake model captures well both the wake shape and maximum velocity deficit. In contrast, the Gaussian model estimates well the velocity deficit in the centre of the wake but is unable to reproduce the wake shape. The profiles at $x/D = 3$ show that both models underestimate the velocity deficit at this location. At $x/D \geq 5$, the super-Gaussian model agrees well with the LES results, while the Gaussian model underestimates the velocity deficit magnitude, except for $x/D = 9$ in which there is a good agreement.

The results for case 1b with $\xi = 2.0$ are presented in Figure 4 at the same downstream sections as in Figure 3, with the profiles nearer to the VAT exhibiting a more pronounced top-hat distribution. Compared to LES, a larger wake width is predicted by the super-Gaussian model at $x/D = 1$, likely due to an over-estimation of the initial wake width value ε (similarly to the results obtained in the Gaussian model derivation for HATs by Bastankhah & Porté-Agel (2014) in which a one-fifth reduction of ε yielded better results), or from the influence of the proximity of the turbine bottom tip to the ground surface that generates flow acceleration ($\Delta U \leq 0$) which is not captured in the wake models. Nevertheless, the super-Gaussian model yields a good prediction of the wake width in the vertical profiles further downstream as well as in the rest of the cases analysed, i.e. captures well the wake evolution over the horizontal and vertical directions. In cases 1a and 1b, an uneven wake shape is observed in the far wake at $x/D = 9$, agreeing with the evolution of the ratio n_z/n_y presented in Figure 2, with a symmetric (or circular) wake shape attained at $x/D \approx 16$ and 32 for $\xi = 1.0$ and 2.0, respectively.

Case 1c considers a turbine with a small aspect ratio of 0.25, i.e. the VAT rotor's height is four times smaller than its diameter. Wake predictions from our theoretical models presented in Figure 5 evidence that the super-Gaussian model is able to accurately predict the near and far wakes. However, the Gaussian model underestimates the maximum velocity deficit in the near wake for $x/D \leq 3$ but attains a good accuracy further downstream as the wake becomes nearly symmetric after $x/D = 7$, in agreement with Figure 2. The presented results show that VAT wakes evolve from an elliptical distribution to a circular one. This is observed in Figure 6, with contours of velocity deficit over yz-planes at several

Figure 5. *Normalised velocity deficit profiles for case 1c with C_T = 0.80 and ξ = 0.25. Same legend as* Figure 3.

Figure 6. *Velocity deficit contours over yz-planes at various streamwise locations for cases 1a (top) and 1b (bottom) which depict the evolution of the wake from an elliptical to a circular shape, as indicated in* Figure 2. *Shaded area represents the VAT rotor's cross-section.*

streamwise locations for cases 1a (ξ = 1.0) and 1b (ξ = 2.0), only showing values of $\Delta U/U_0 \geq 0.05$. With ξ = 1.0, the wake immediately downstream of the turbine remains wider in the vertical direction. At x/D = 2, its shape is almost symmetric whilst at x/D = 5 the wake has a larger extent in the transverse direction, reaching an almost circular shape at $10D$. As per the case with ξ = 2.0, the wake is highly three-dimensional at all locations, progressively evolving towards a circular shape.

4.2. Case 2: VATs with Varying C_T from Abkar & Dabiri (2017)

We now consider another LES set-up comprising a single VAT with D = 26 m and H = 24 m, i.e. ξ = 0.92, operating at TSRs, λ, of 3.8 (case 2a) and 2.5 (case 2b). In these operating conditions, the VAT yields C_T equal to 0.64 and 0.34, and we are interested in comparing these as VAT wakes develop
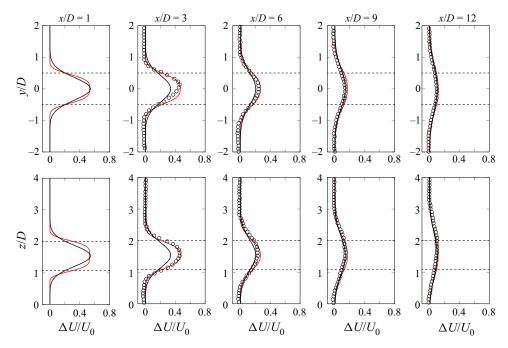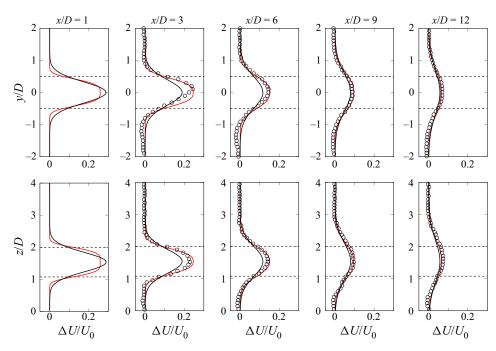
Figure 7. *Normalised velocity deficit profiles for case 2a with C_T = 0.64, λ = 3.8 and ξ = 0.92. Comparison of our proposed super-Gaussian (red line) and Gaussian (black line) analytical wake models, with the LES results from* Abkar & Dabiri (2017) *(circles).*

a different dynamics depending on λ. Furthermore, in case 2c the turbine has a C_T equal to 0.64 and operates at λ = 3.8, as in case 1a, but with ξ = 1.85. Turbines are equipped with three NACA 0018 blades with a chord length c = 0.75 m.
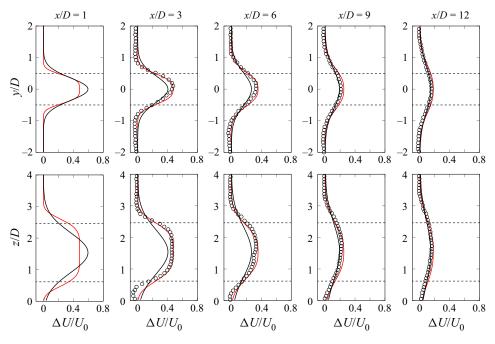
The validation of normalised velocity deficit predictions obtained with our analytical wake models compared with LES results from Abkar & Dabiri (2017) are presented in Figure 7 with horizontal and vertical profiles across the turbine wake centre at x/D = 1, 3, 6, 9 and 12. Immediately downstream the VAT, at x/D = 1.0, the super-Gaussian model is able to capture the three-dimensional wake with the Gaussian model predicting a narrower wake core. At x/D = 3, the super-Gaussian model achieves excellent agreement with the LES data whilst the Gaussian model slightly under-predicts $\Delta U/U_0$ in both vertical and horizontal profiles. At locations further downstream, both models predict well the velocity deficit.

Figure 8 presents the results obtained for case 2b in which the VAT has a lower C_T than cases 2a and 2c. The super-Gaussian model again attains a good velocity field prediction at all locations, notably improving the velocity estimates from the Gaussian model, especially at x/D = 3 and 6, but both provide a reasonable agreement of the wake width. Due to the low C_T in case 2b, the wake shape features an almost Gaussian distribution over the horizontal and vertical directions already at $x/D \geq 6$, which supports the self-similarity assumption in the Gaussian shape distribution and thus both theoretical models achieve a great accuracy.

The turbine in case 2c has almost the same aspect ratio as in case 1b but with a lower thrust coefficient, which would lead to a faster wake recovery. Profiles of velocity deficit are shown in Figure 9 evidencing the accuracy of the super-Gaussian model in capturing the velocity deficit magnitude and its shape throughout the wake, notably improving the Gaussian model's prediction in the near wake at x/D = 3. The wake is observed to expand unevenly over the vertical and horizontal directions as in Figure 4, but the wake recovery is faster for C_T = 0.64 than with C_T = 0.80, as would be expected.

Figure 8. *Normalised velocity deficit profiles for case 2b with $C_T = 0.34$, $\lambda = 2.5$ and $\xi = 0.92$. Same legend as Figure 7.*

Figure 9. *Normalised velocity deficit profiles for case 2c with $C_T = 0.64$, $\lambda = 3.8$ and $\xi = 1.85$. Same legend as in Figure 7.*
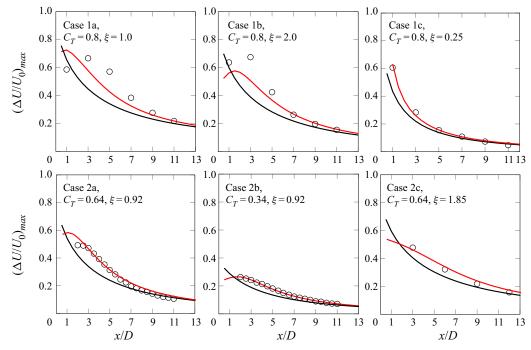
Figure 10. *Evolution of the maximum normalised maximum velocity deficit in the streamwise direction for all cases analysed. Comparison of our proposed super-Gaussian (red line) and Gaussian (black line) wake models, with the LES results (circles) from Shamsoddin & Porté-Agel (2020) in cases 1a to 1c and Abkar & Dabiri (2017) in cases 2a to 2c.*

4.3. Prediction of the Velocity Scale

To summarise the accuracy of our theoretical models in terms of the predictions of VAT wakes for the six cases analysed in comparison to LES results, the values of maximum velocity deficits in the streamwise direction are presented in Figure 10, which represents the velocity scale in the theoretical models (15). Overall, the super-Gaussian model attains an excellent agreement with LES in cases 1c, 2a, 2b and 2c over the whole wake length, whilst for cases 1a and 1b there is an underestimation of the velocity deficit until $x/D \approx 5$, as a consequence of the models over-predicting the wake width (see Figure 7). The Gaussian model consistently provides good estimates of ΔU in the far wake but fails to achieve a good agreement in the near wake. Whilst further improvement in cases 1a and 1b would be obtained tuning the super-Gaussian parameters, we aimed at building a consistent model with a given set of parameters that yields the best predictions for the six benchmarks together. A further advantage of our Gaussian model is that the proposed initial wake width (20) enables the calculation of the velocity field in all the wake region, overcoming the limitations from previous models (Abkar, 2019) that could not provide physical estimates in the near wake for ranges of C_T values.

5. Conclusions

We present a new set of theoretical super-Gaussian and Gaussian models for vertical axis wind and hydro-kinetic turbine (VAT) wakes that capture their intrinsic three-dimensional shape. Our super-Gaussian model is based on the superposition of two super-Gaussian shape functions that evolve in the downstream direction according to the exponents n_y and n_z which scale with the rotor's diameter (D) and height (H), respectively. This model represents well the nearly top-hat near-wake shape and elliptical distribution found along most of the wake length until it eventually collapses into an axisymmetric circular shape.

Figure 11. *Evolution of the super-Gaussian coefficients n_z and n_y in the downstream direction for various aspect ratios $\xi = H/D$.*

The ratio between the shape function exponents indicates the degree of horizontal-to-vertical wake shape asymmetry (which varies with the rotor's height-to-diameter aspect ratio ($\xi = H/D$) but is invariant to the flow conditions) showed that the fastest recovery to an axisymmetric wake was obtained for $\xi = 1.5$ at a distance of $8D$ downstream. Our Gaussian model considers the wake to be self-similar and yielded reliable estimates of the initial wake width but was less accurate in the near-wake representation than its super-Gaussian counterpart. In both models the wake width increases linearly as a function of turbulence intensity at the same rate in the vertical and transverse directions.

We validated the accuracy of our models with high-fidelity LES data in six cases involving a standalone VAT with varying thrust coefficients and aspect ratios. Our models captured the three-dimensional wake distribution, yielding good estimates of the maximum velocity deficit, with the super-Gaussian model providing the best predictions. The transition from an elliptical to a circular Gaussian shape is well captured by the super-Gaussian model, which indicated this is attained at a downstream location depending on the VAT's rotor aspect ratio, in line with the results previously observed in the LES. The presented results confirm the accuracy and reliability of our super-Gaussian model in the prediction of VAT wakes both in the near and far regions, while our Gaussian model represents well the far wake.

Appendix

As VAT wakes have two length scales, namely H and D, that determine their shape, in Figure 11 we show the change in the super-Gaussian coefficients n_z and n_y (8) with downstream distance. At x/D, both coefficients reach their maxima ($n_z = 6.9$ and $n_y = 3.35$) corresponding to the most top-hat-like shape, then decaying exponentially until the Gaussian shape of exponent 2.4. We observe that for $\xi \leq 1.5$ the vertical wake shape eventually evolves quicker to the limit value of 2.4, whilst above that value the wake always recovers the Gaussian distribution faster over the horizontal y-direction. In Figure 2 we characterised the wake asymmetry as the ratio n_z/n_y, which attained a maximum value at the wake onset ($x/D = 0$) except when $\xi \geq 4.0$ when this is achieved shortly downstream from the turbine. Figure 11 indicates that the latter happens because the wake in the lateral direction (n_y) changes more rapidly from the initial top-hat to the Gaussian shape than over the vertical direction.

References

Abkar, M. (2019). Theoretical modeling of vertical-axis wind turbine wakes. *Energies*, *12*(1), 10.

Abkar, M., & Dabiri, J. O. (2017). Self-similarity and flow characteristics of vertical-axis wind turbine wakes: An LES study. *Journal of Turbulence*, *18*(4), 373–389.

Araya, D., Colonius, T., & Dabiri, J. O. (2017). Transition to bluff-body dynamics in the wake of vertical-axis wind turbines. *Journal of Fluid Mechanics*, *813*, 346–381.

Archer, C. L., Vasel-Be-Hagh, A., Yan, C., Wu, S., Pan, Y., Brodie, J. F., & Maguire, A. E. (2018). Review and evaluation of wake loss models for wind energy applications. *Applied Energy*, *226*, 1187–1207.

Bachant, P., & Wosnik, M. (2016). Effects of Reynolds number on the energy conversion and near-wake dynamics of a high solidity vertical-axis cross-flow turbine. *Energies*, *9*(2), 73.

Bastankhah, M., & Porté-Agel, F. (2014). A new analytical model for wind-turbine wakes. *Renewable Energy*, *70*, 116–123.

Bastankhah, M., & Porté-Agel, F. (2016). Experimental and theoretical study of wind turbine wakes in yawed conditions. *Journal of Fluid Mechanics*, *806*, 506–541.

Blondel, F., & Cathelain, M. (2020). An alternative form of the super-Gaussian wind turbine wake model. *Wind Energy Science*, *5*(3), 1225–1236.

Castro-Santos, T., & Haro, A. (2013). Survival and behavioral effects of exposure to a hydrokinetic turbine on juvenile Atlantic salmon and adult American shad. *Estuaries and Coasts*, *38*, 203–214.

Frandsen, S., Barthelmie, R., Pryor, S., Rathmann, O., Larsen, S., Højstrup, J., & Thøgersen, M. (2006). Analytical modelling of wind speed deficit in large offshore wind farms. *Wind Energy*, *9*, 39–53.

Hezaveh, S. H., Bou-Zeid, E., Dabiri, J., Kinzel, M., Cortina, G., & Martinelli, L. (2018). Increasing the power production of vertical-axis wind-turbine farms using synergistic clustering. *Boundary-Layer Meteorology*, *169*, 275–296.

Kadum, H., Friedman, S., Camp, E. H., & Bayoán Cal, R. (2018). Development and scaling of a vertical axis wind turbine wake. *Journal of Wind Engineering and Industrial Aerodynamics*, *174*, 303–311.

Massie, L., Ouro, P., Stoesser, T., & Luo, Q. (2019). An actuator surface model to simulate vertical axis turbines. *Energies*, *12*(24), 4741.

Mendoza, V., Chaudhari, A., & Goude, A. (2019). Performance and wake comparison of horizontal and vertical axis wind turbines under varying surface roughness conditions. *Wind Energy*, *22*(4), 458–472.

Meneveau, C. (2019). Big wind power: Seven questions for turbulence research. *Journal of Turbulence*, *20*(1), 2–20.

Ouro, P., Runge, S., Luo, Q., & Stoesser, T. (2019). Three-dimensionality of the wake recovery behind a vertical axis turbine. *Renewable Energy*, *133*, 1066–1077.

Ouro, P., & Stoesser, T. (2017). An immersed boundary-based large-eddy simulation approach to predict the performance of vertical axis tidal turbines. *Computers & Fluids*, *152*, 74–87.

Ouro, P., Stoesser, T., & Ramírez, L. (2018). Effect of blade cambering on dynamic stall in view of designing vertical axis turbines. *ASME Journal of Fluids Engineering*, *140*(6), 061104.

Porté-Agel, F., Bastankhah, M., & Shamsoddin, S. (2020). Wind-turbine and wind-farm flows: A review. *Boundary-Layer Meteorology*, *174*, 1–59.

Posa, A. (2020a). Dependence of the wake recovery downstream of a Vertical Axis Wind Turbine on its dynamic solidity. *Journal of Wind Engineering and Industrial Aerodynamics*, *202*, 104212.

Posa, A. (2020b). Influence of tip speed ratio on wake features of a vertical axis wind turbine. *Journal of Wind Engineering and Industrial Aerodynamics*, *197*, 104076.

Posa, A., & Balaras, E. (2018). Large eddy simulation of an isolated vertical axis wind turbine. *Journal of Wind Engineering and Industrial Aerodynamics*, *172*, 139–151.

Rolin, V., & Porté-Agel, F. (2018). Experimental investigation of vertical-axis wind-turbine wakes in boundary layer flow. *Renewable Energy*, *118*, 1–13.

Ross, H., & Polagye, B. (2020). An experimental evaluation of blockage effects on the wake of a cross-flow current turbine. *Journal of Ocean Engineering and Marine Energy*, *6*, 263–275.

Shamsoddin, S., & Porté-Agel, F. (2016). A large-eddy simulation study of vertical axis wind turbine wakes in the atmospheric boundary layer. *Energies*, *9*(5), 366.

Shamsoddin, S., & Porté-Agel, F. (2020). Effect of aspect ratio on vertical-axis wind turbine wakes. *Journal of Fluid Mechanics*, *889*, R1.

Shapiro, C. R., Starke, G. M., Meneveau, C., & Gayme, D. F. (2019). A wake modeling paradigm for wind farm design and control. *Energies*, *12*, 2956.

Stallard, T., Feng, T., & Stansby, P. K. (2015). Experimental study of the mean wake of a tidal stream rotor in a shallow turbulent flow. *Journal of Fluids and Structures*, *54*, 235–246.

Stansby, P. K., & Stallard, T. (2016). Fast optimisation of tidal stream turbine positions for power generation in small arrays with low blockage based on superposition of self-similar far-wake velocity deficit profiles. *Renewable Energy*, *92*, 366–375.

Tennekes, H., & Lumley, J. (1972). *A first course in turbulence*. Cambridge, MA: The MIT press.

Tescione, G., Ragni, D., He, C., Simão Ferreira, C. J., & van Bussel, G. (2014). Near wake flow analysis of a vertical axis wind turbine by stereoscopic particle image velocimetry. *Renewable Energy*, *70*, 47–61.